IEEE Access
Multidisciplinary | Rapid Review | Open Access Journal

Received December 24, 2018, accepted January 7, 2019, date of publication January 14, 2019, date of current version February 14, 2019.

Digital Object Identifier 10.1109/ACCESS.2019.2892746

Electrical Vehicle Path Tracking Based Model Predictive Control With a Laguerre Function and Exponential Weight

BING ZHANG[1], CHANGFU ZONG[1], GUOYING CHEN[1], AND BANGCHENG ZHANG[2]
[1]Department of State Key Laboratory of Automotive Simulation and Control, Jilin University, Changchun 130022, China
[2]Automotive Engineering Research Institute, Changchun University of Technology, Changchun 130012, China

Corresponding authors: Changfu Zong (zongcf@jlu.edu.cn) and Bangcheng Zhang (zhangbangcheng@ccut.edu.cn)

This work was supported in part by the National Natural Science Foundation of China under Grant 61751304, Grant 51575224, and Grant 51505178, and in part by the China Postdoctoral Science Foundation under Grant 2014M561289.

ABSTRACT Model predictive control (MPC) is advantageous for designing an electrical vehicle path-tracking controller, but the high computational complexity, mathematical problem, and parameterization challenge adversely affect the control performance. Hence, based on a fully actuated-by-wire electrical vehicle (FAW-EV), a novel path-tracking controller based on improved MPC with a Laguerre function and exponential weight (LEMPC) is designed. The massive optimization control parameters of MPC with a long control horizon are reduced by introducing a fitting orthogonal sequence consisting of Laguerre functions, thereby substantially reducing the computational complexity without sacrificing the tracking accuracy. An exponential weight with decreasing characteristic is introduced to MPC to solve the mathematical problem, thereby improving the robustness of the path tracking controller. In addition, the parameterization access for online adjusting path tracking control performance can be provided by the proposed method. The path tracking motion realization for FAW-EV is subsequently illustrated. Finally, several simulations are implemented to verify the advantages of the proposed method.

INDEX TERMS Path track, electrical vehicle, model predictive control (MPC), Laguerre function, exponential weight.

I. INTRODUCTION

In the development of sensing, wire-control, and electricity-storage capacities, the autonomous electrical vehicle has attracted considerable attention because of its convenience, intelligence and environmental protection [1]– [3], and an increasing number of researchers are focusing on this advanced device. The driving control method is the core of the autonomous electric vehicle; its control task can often be functionally divided into path planning and path tracking [4], with the relationship shown in Fig. 1. Path tracking control is very significant since it is the cornerstone for realizing autonomous driving of electrical vehicles [5]– [8].

The primary target of a path tracking control system is to control the vehicle to accurately follow a reference path given by path planning. This process is not easy due to the requirement of simultaneously ensuring tracking accuracy and vehicle dynamic stability [9]– [11]. For this function, many control methods have been applied, such as slide mode control (SMC) [12]– [14], robust control [15], [16], model predictive control (MPC) [17], [18], linear quadratic regulator (LQR) optimal control [19], and output constraint control [20]. Each of these technologies can converge the vehicle trajectory to the expectations, especially, MPC is more suitable since the constrained mechanism can take the vehicle dynamic limit into consideration, and the control input for path tracking can be achieved concerning overall situation during prediction horizon [21], [22].

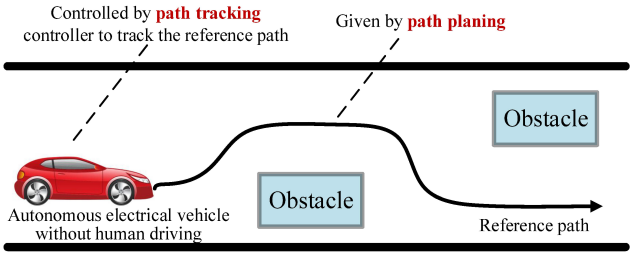

FIGURE 1. Relationship between autonomous driving control tasks.

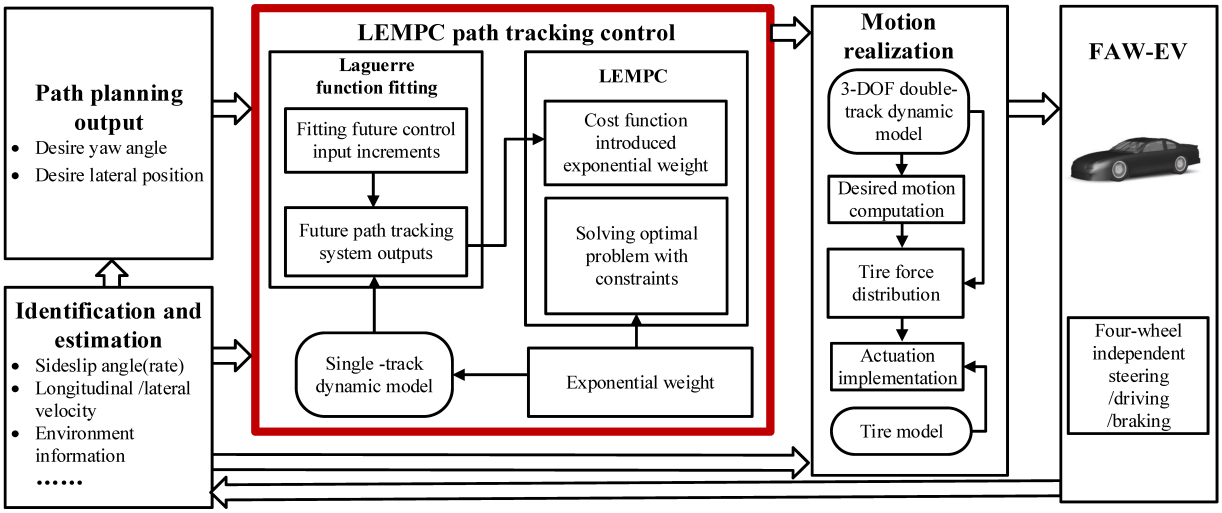

FIGURE 2. Complete control structure for autonomous driving of the FAW-EV.

The essential idea of MPC is to achieve control input by solving the optimization problem of minimizing the error between the future system output and reference output, although this is only a basic control framework, and many researchers revise it to meet different path tracking control requirements. For tracking the planned collision-avoiding path, multiple constraints are introduced to the MPC framework in [4] to track a reference path that minimizes the possibility of collision. In [23], an electrical vehicle path tracking controller based on the MPC framework is proposed in which the steering angle and wheel slip ratio are the control inputs. Reference [24] combines the MPC and SMC to robustly track a reference path; this study mainly addresses the micro-vehicle, and the tire stability limit is considered to harmonize the path tracking accuracy and vehicle robustness. For path tracking control of wheeled robots, reference [25] proposes a backstepping kinematic controller based MPC with dual heuristic programming.

However, the basic framework of above MPC path tracking controllers encounters its limits in practical applications of electrical vehicle path tracking. First, the long control horizon is always introduced to ensure the favorable tracking control performance. Consequently, the optimization problem of MPC possesses massive optimization control parameters defined as future control inputs or future control input increments. Therefore, a high computational complexity arises and can be made worse under multiple dimensions of control inputs and constraints. Second, there is a mathematical problem in MPC in that the instability of the predictive plant is cumulated during predicting future system outputs, which leads to high sensitivity even to slight disturbances. Such unexpected sensitivity will be deteriorated by setting a long prediction horizon, however, which is always necessary for the dynamic-unstable driving conditions of electrical vehicle path tracking. Finally, the control requirement for path tracking control performance is varied as different driving conditions; unfortunately, the MPC parameters that significantly influence the path tracking control performance are very difficult to adjust finely online.

The previous studies show that the MPC controller with Laguerre fitting can reduce the computational complexity of MPC optimization problem [26], and the unexpected sensitivity of MPC can be improved by introducing exponential weight [27], therefore, motivated by the problems exited in MPC path tracking controller, a novel path tracking controller based on improved MPC with a Laguerre function and exponential weight (LEMPC) is designed for the fully actuated-by-wire electrical vehicle (FAW-EV), in which the four wheels can be independently steered, driven and braked [28]. The main contributions of this paper are listed as follows:

(1) In the prediction of future system outputs within MPC path tracking controller, a Laguerre function orthogonal sequence is employed to fit the long control input trajectory by a linearized combination; therefore, the computational complexity can be reduced without sacrificing the tracking performance by transforming the optimization control parameters from massive control input increments to a few fitting coefficients.

(2) The mathematical problem inherent in MPC is analyzed and solved by introducing an exponential weight to the cost function of the MPC path tracking controller; therefore, the unexpected sensitivity of the MPC path tracking controller with a long prediction horizon can be ameliorated, and the path tracking control robustness can be improved.

(3) We propose an LEMPC path tracking control method in which the attenuating property diversity of a Laguerre function orthogonal sequence with different parameters provides parameterization for finely online-adjusting path tracking control performance to varied path tracking requirements; the prediction horizon can be adjusted online to variations in the vehicle dynamic stability since the mathematical problem is improved. Moreover, the parameterized path tracking

controller basing LEMPC can be adjusted to compensate the linearized error.

For convenient and flexible control, the autonomous driving control system of an FAW-EV is based on a modularized structure, as shown as Fig. 2. This paper emphasizes the LEMPC path tracking controller design, which is illustrated as follows: Section II gives both the predictive plant for LEMPC path tracking control and the model capturing the FAW-EV dynamic characteristics. Section III illustrates the improved path tracking control method based on LEMPC, and the realization of path tracking motion with the FAW-EV is briefly discussed. Section IV validates the availabilities of the proposed method by several simulations, and the main ideas for adjusting the parameters are given in this section. Finally, a succinct conclusion is given in section V.

II. PREDICTIVE PLANT AND DYNAMIC MODEL

A. PREDICTIVE PLANT FOR LEMPC PATH TRACKING

For LEMPC, a predictive plant is employed to predict future system outputs [29], [30]. In this paper, the single-track vehicle model is introduced to build the predictive plant. As shown in Fig. 3, the model ignores the vertical, pitch and roll motions, and the sideslip angles of the left wheels are assumed to be equal to those of right [31]. For generality, the model is considered under the condition of a small front steering angle. The desired tracking motion is described by front steering angle, therefore the rear steering angle is assumed to be 0, with the given initial value of V_x set to desired longitudinal velocity. Combining with the stiffness tire model, and according to Newton law, the predictive plant is described as

$$\begin{cases} m\dot{V}_y = -mV_x\dot{\psi} + 2[C_{cf}(\delta_{fd} - \frac{V_y + l_f\dot{\psi}}{V_x}) \\ \qquad + C_{cr}\frac{l_r\dot{\psi} - V_y}{V_x}] \\ m\dot{V}_x = mV_y\dot{\psi} + 2[C_{lf}s_f + C_{cf}(\delta_{fd} \\ \qquad - \frac{V_y + l_f\dot{\psi}}{V_x})\delta_{fd} + C_{lr}s_r] \\ I_z\ddot{\psi} = 2\,[l_fC_{cf}(\delta_{fd} - \frac{V_y + l_f\dot{\psi}}{V_x}) - l_rC_{cr}\frac{l_r\dot{\psi} - V_y}{V_x}] \\ \dot{Y} = V_x\sin\psi + V_y\cos\psi \\ \dot{X} = V_x\cos\psi - V_y\sin\psi \end{cases} \tag{1}$$

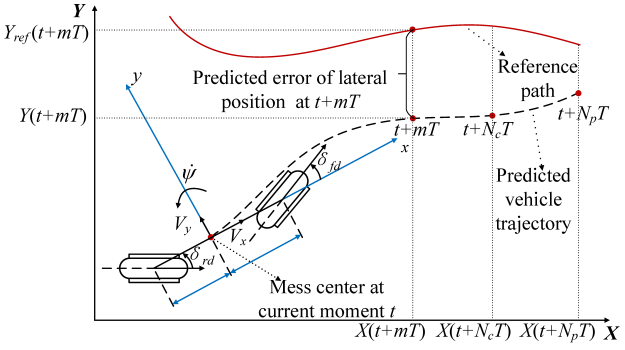

FIGURE 3. Predictive plant based single-track vehicle model.

where X and Y denote the vehicle longitudinal position and lateral position, respectively, C_{lf} and C_{lr} denote the front and rear equivalent longitudinal cornering stiffness, respectively, C_{cf} and C_{cr} denote the front and rear equivalent lateral cornering stiffness, respectively, s_f and s_r denote the front and rear longitudinal slip rates, respectively, ψ denotes the yaw angle, and V_x and V_y denote the longitudinal and lateral vehicle velocities, respectively. δ_{fd} denotes the desired front steering angle.

MPC method is computationally complicated, and the nonlinearity of the predictive plant aggravates the computational burden. Previous studies show that formulating the vehicle dynamic linearly combining with a quadratic cost function can reduce the computational effort and improve the efficiency [32], [33]. Therefore, the plant (1) is linearized around current vehicle states $x(t)$ and previous control input $u(t-1)$ with assumption that the control input is unchangeable within prediction horizon [33], and the achieved time-varied form as

$$\begin{cases} \dot{x} = A_t x(t) + B_t u(t) \\ y = C_t x(t) \end{cases} \tag{2}$$

with the vehicle state vector $x = \left[V_x, V_y, \psi, \dot{\psi}, Y, X\right]^T$, choosing the control input u as δ_{fd}, which is used to describe the desired tracking motion, and the brake and propulsion are not concerned in path tracking controller. A_t and B_t are system matrices. In the path tracking system, we divide the path tracking control issue into yaw angle tracking and lateral position tracking; the system output is $y = [\psi, Y]^T$, and the system output matrix C_t is therefore

$$C_t = \begin{bmatrix} 0 & 0 & 1 & 0 & 0 & 0 \\ 0 & 0 & 0 & 0 & 1 & 0 \end{bmatrix}$$

Predictive plant is used to predict future vehicle states as well as future system outputs, for reducing the linearized error, a simple compensation is given in formulation of MPC optimal problem described in part A of next section.

Significantly, the predictive plant is used only to describe the future tracking error between the vehicle motion and the desired motion according reference path. Since the wheel steering angels of FAW-EV are controlled independently, the control input δ_{fd} of (2) is used only to describe the desired path tracking motion and subsequently transformed to tire forces of four wheels.

B. DYNAMIC MODEL FOR FAW-EV MOTION REALIZATION

For realizing path tracking motion with the FAW-EV, the relationships among the vehicle integral motions, total efforts, and tire forces are captured by the double-track model with 3 degrees of freedom (DOFs), which takes only the planar motion into consideration. As shown in Fig. 4(a), the dynamic characteristics for the longitudinal, lateral and yaw directions

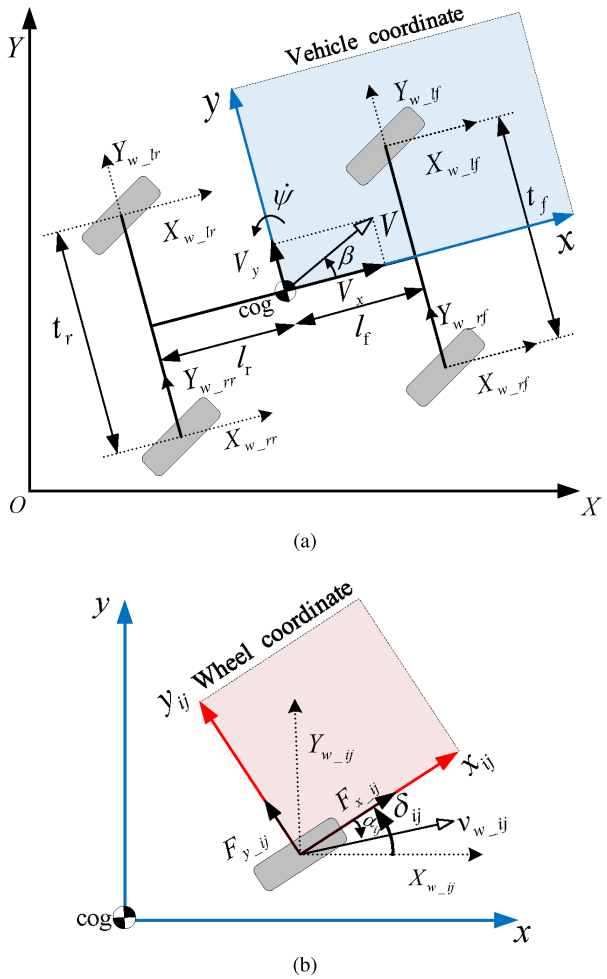

FIGURE 4. Schematic of the FAW-EV dynamic model: (a) Integral vehicle dynamic. (b) Single wheel dynamic.

are described as

$$\begin{cases} a_x = \dot{V}_x - \dot{\psi} V_y = \frac{1}{m} F_{xd} = \frac{1}{m} \sum_{i=l}^{r} \sum_{j=f}^{r} X_{w\_ij} \\ a_y = \dot{V}_y + \dot{\psi} V_x = \frac{1}{m} F_{yd} = \frac{1}{m} \sum_{i=l}^{r} \sum_{j=f}^{r} Y_{w\_ij} \\ M_{zd} = I_z \ddot{\psi} = \frac{t_f}{2} \left(X_{w\_rf} - X_{w\_lf} \right) + \frac{t_r}{2} \left(X_{w\_rr} - X_{w\_lr} \right) \\ \quad + l_f \left(Y_{w\_lf} + Y_{w\_rf} \right) - l_r \left(Y_{w\_lr} + Y_{w\_rr} \right) \end{cases} \tag{3}$$

where the total efforts of F_{xd}, F_{yd}, and M_{zd} are the vehicle longitudinal force, lateral force, and vehicle yaw torque, respectively. I_z denotes the rotary inertia of the vehicle around the vehicle vertical axle. X_{w_ij} and Y_{w_ij} denote the longitudinal and lateral tire forces, respectively, acting on the point between the tire and ground in the vehicle-body coordinate system, and they can be described as

$$\begin{cases} X_{w\_ij} = F_{x\_ij} \cos \delta_{ij} - F_{y\_ij} \sin \delta_{ij} \\ Y_{w\_ij} = F_{x\_ij} \sin \delta_{ij} + F_{y\_ij} \cos \delta_{ij} \end{cases} \quad \forall i \in \{l, r\}, \forall j \in \{f, r\} \tag{4}$$

where F_{x_ij} and F_{y_ij} denote the longitudinal and lateral tire forces, respectively, acting on the center of the tire and δ_{ij} denotes the wheel steering angle, as shown in Fig. 4(b).

For realizing the desired lateral tire force, the empirical relation curve between the tire sideslip angle α_{ij} and the lateral tire force F_{y_ij} is fitted by the arctangent function [34]:

$$F_{y\_ij} = -C_{\alpha\_ij} \sqrt{1 - \left(\frac{F_{x\_ij}}{\mu_{ij} F_{z\_ij}} \right)^2} \frac{\mu_{ij}}{k_{ij}} \tan^{-1} \left(\frac{k_{ij}}{\mu_{ij}} \alpha_{ij} \right) \tag{5}$$

where $k_{ij} = C_{\alpha\_ij} \pi / p F_{z\_ij}$ and the value of curve-fitting constant p is set as 2.9 to improve the fitting accuracy under a relatively large sideslip angle. μ_{ij} denotes the tire-road friction factor of each wheel, and a large μ_{ij} often gives a high dynamic stability margin. F_{z_ij} denotes the tire vertical load, which can be achieved by referencing [35]. Angle σ_{ij} between the velocity of the wheel center and the longitudinal axle of the vehicle body is defined as $\sigma_{ij} = \alpha_{ij} + \delta_{ij}$ and computed by

$$\begin{cases} \sigma_{lf,rf} = \tan^{-1} \left(\left(V_y + l_f \dot{\psi} \right) / \left(V_x \mp t_f \dot{\psi} / 2 \right) \right) \\ \sigma_{lr,rr} = \tan^{-1} \left(\left(V_y - l_r \dot{\psi} \right) / \left(V_x \mp t_r \dot{\psi} / 2 \right) \right) \end{cases} \tag{6}$$

where the sign "$\mp$" refers to the left/right wheel.

III. PARTH TRACKING CONTROL BASED LEMPC

The basic idea of the LEMPC path tracking controller is that a Laguerre function orthogonal sequence is employed to fit the trajectory of future control input increments within the MPC path tracking optimization problem. In addition, an exponential weight is introduced to the path tracking cost function to solve the mathematical problem. The control principle is shown in Fig. 5. This improved method is based on the MPC path tracking control framework, whose illustration is shown at the beginning of this section.

A. BASIC MPC FRAMEWORK FOR PATH TRACKING

An integrator is introduced to converge the steady-state error to zero, and the control input of the MPC path tracking controller is therefore changed to the incremental form Δu. With a discrete time step of T, plant (2) can be discretized as follows:

$$\begin{cases} \xi(k+1|t) = \tilde{A}_{k,t} \xi(k|t) + \tilde{B}_{k,t} \Delta u(k|t) \\ y(k|t) = \tilde{C}_{k,t} \xi(k|t) \end{cases} \tag{7}$$

where augmented state matrix

$$\xi(k|t) = \left[x(k|t) \;\; u(k-1|t) \right]^T$$

and

$$\tilde{A}_{k,t} = \begin{bmatrix} I + TA_t & TB_t \\ O_{m \times n} & I_m \end{bmatrix}$$

$$\tilde{B}_{k,t} = \begin{bmatrix} TB_t \\ I_m \end{bmatrix}$$

$$\tilde{C}_{k,t} = \begin{bmatrix} 0\,0\,1\,0\,0\,0\,0 \\ 0\,0\,0\,0\,1\,0\,0 \end{bmatrix}$$

With (7), the predicted future system outputs within the prediction horizon can be achieved by

$$Y_{sys}(k) = \Psi_k \xi(k|t) + \Theta_k \Delta U(k|t) \tag{8}$$

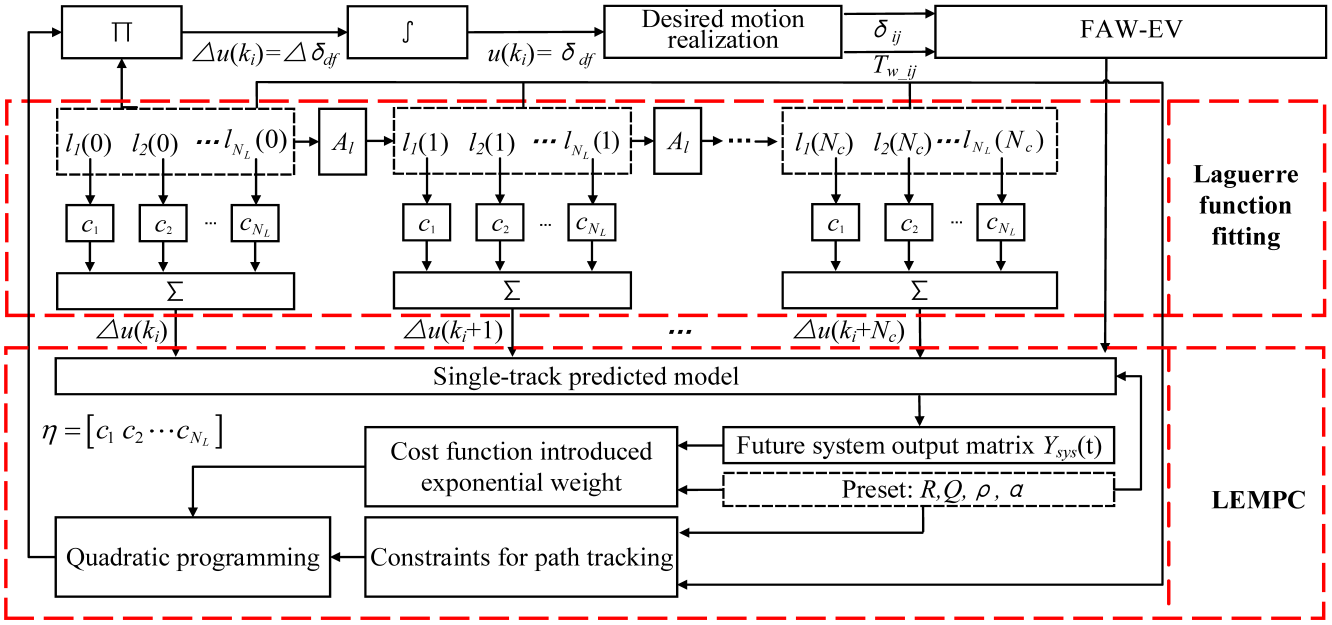

FIGURE 5. Schematic diagram of the LEMPC path tracking controller.

where

$$Y_{sys}(k)_{(N_p\times 1)} = \begin{bmatrix} y(k+1|t) \\ y(k+2|t) \\ \cdots \\ y(k+N_c|t) \\ \cdots \\ y(k+N_p|t) \end{bmatrix} \quad \Psi_{k(N_p\times 1)} = \begin{bmatrix} \tilde{C}_{k,t}\tilde{A}_{k,t} \\ \tilde{C}_{k,t}\tilde{A}_{k,t}^2 \\ \cdots \\ \tilde{C}_{k,t}\tilde{A}_{k,t}^{N_c} \\ \cdots \\ \tilde{C}_{k,t}\tilde{A}_{k,t}^{N_p} \end{bmatrix}$$

$$\Theta_{k(N_p\times N_c)} = \begin{bmatrix} \tilde{C}_{k,t}\tilde{B}_{k,t} & 0 & 0 & 0 \\ \tilde{C}_{k,t}\tilde{A}_{k,t}\tilde{B}_{k,t} & \tilde{C}_{k,t}\tilde{B}_{k,t} & 0 & 0 \\ \cdots & \cdots & \ddots & \cdots \\ \tilde{C}_{k,t}\tilde{A}_{k,t}^{N_c-1}\tilde{B}_{k,t} & \tilde{C}_{k,t}\tilde{A}_{k,t}^{N_c-2}\tilde{B}_{k,t} & \cdots & \tilde{C}_{k,t}\tilde{B}_{k,t} \\ \tilde{C}_{k,t}\tilde{A}_{k,t}^{N_c}\tilde{B}_{k,t} & \tilde{C}_{k,t}\tilde{A}_{k,t}^{N_c-1}\tilde{B}_{k,t} & \cdots & \tilde{C}_{k,t}\tilde{A}_{k,t}\tilde{B}_{k,t} \\ \vdots & \vdots & \ddots & \vdots \\ \tilde{C}_{k,t}\tilde{A}_{k,t}^{N_p-1}\tilde{B}_{k,t} & \tilde{C}_{k,t}\tilde{A}_{k,t}^{N_p-2}\tilde{B}_{k,t} & \cdots & \tilde{C}_{k,t}\tilde{A}_{k,t}^{N_p-N_c-1}\tilde{B}_{k,t} \end{bmatrix}$$

$$\Delta U(k)_{(N_c\times 1)} = \begin{bmatrix} \Delta u(k|t) \\ \Delta u(k+1|t) \\ \cdots \\ \Delta u(k+N_c-1|t) \end{bmatrix}$$

where N_p and N_c represent the lengths of the prediction horizon and control horizon, respectively.

The control objective for path tracking can be expressed as the followed optimization control problem with a receding horizon.

$$min\ J = \sum_{i=1}^{N_p} \left\| y_{ref}(k+i) - y(k+i) \right\|_Q^2 \tag{9a}$$

$$+ \sum_{i=0}^{N_c-1} \left\| \Delta u(k+i) \right\|_R^2 + \rho\, \varepsilon^2$$

$$s.t.\ \Delta U_{min} \le \Delta U(k) \le \Delta U_{max} \tag{9b}$$

$$U_{min} \le U \le U_{max} \tag{9c}$$

$$Y_{min} \le Y_{sys} \le Y_{max} \tag{9d}$$

where y_{ref} is the reference output and consists of the reference yaw angle ψ_{ref} and reference lateral position Y_{ref}. Q and R are weights for the system outputs and control input increments, respectively. With the first term in the cost function (9a), the predictive errors between the predicted system outputs and future reference outputs are penalized through a weighted norm. This approach ensures that the vehicle tracks the reference path as accurately as possible. The second term of (9a) is a weighted norm on the input increments, which aims to minimize the control effort. The final term of (9a) is a penalty on the slack variable added to avoid the infeasibility under the strict constraints. Large weight of slack variable gives more relaxation to the optimization control problem, however, with sacrificing the path tracking performance; therefore, the slack variable weight can be chosen as a large value only under condition that the optimization control problem is insoluble [36]. Equations (9b)-(9d) describe the constraints for the control input increments according to the tolerances of the path tracking control system outputs and FAW-EV actuators.

In this paper, we omit the constant term of the cost function; the optimization control problem (9) for path tracking is equivalently arranged into quadratic programming (QP) form as

$$min\ J = V^T H_k V + G_k V \tag{10a}$$

$$s.t.\ \Delta\tilde{U}_{min} \le \Delta U \le \Delta\tilde{U}_{max} \tag{10b}$$

where (10b) is the integration of (9b)-(9d) and the optimization control parameters defined as $V = [\Delta U, \varepsilon]$ are obtained by solving the QP problem as in (10). The coefficient matrices are defined as

$$H_k = \begin{bmatrix} \Theta_k^T Q\, \Theta_t & 0 \\ 0 & \rho \end{bmatrix} \quad G_k = \begin{bmatrix} 2E_k^T Q\, \Theta_k & 0 \end{bmatrix}$$

where E_k is the matrix consisting of predicted errors between the predicted system outputs and future reference outputs within the prediction horizon. For further ensuring the tracking accuracy, during predicting future system outputs, the linearized error for achieving predictive plant (2) are considered in E_k, which can be described as

$$E_k = Y_{REF} - Y_{sys} - E_{line}$$

where Y_{REF} is the matrix consisting of future reference outputs within prediction horizon, E_{line} is the linearized error matrix of system outputs within prediction horizon and can be achieved by

$$E_{line} = MD_k$$

with the D_k is the matrix about the linearized error d_{k0} at the next time. According to [37], dimension of matrix M depends on the length of prediction horizon, and its elements can be described as

$$M(i,j) = \begin{cases} \tilde{C}_{k,t}\tilde{A}_{k,t}^{i-j}, & j \le i \\ 0, & j > i \end{cases}$$

The dimension of ΔU within V is N_c, and only the first element can be used as a control input by integral action as in (11).

$$u(k) = u(k-1) + \Delta u(k\,|\,t) \tag{11}$$

B. LAGUERRE FUNCTION INTRODUCTION

The principle of reducing the MPC computational complexity is to approximately represent the trajectory of future control input increments $\Delta U(k)$ by linearly combining a sequence of orthogonal functions with few fitting coefficients. Consequently, the whole control horizon can be covered without the need for massive optimization control parameters.

Because of its programming simplicity and favorable approximation ability for variances of the control plant, a Laguerre function orthogonal sequence is chosen as the appropriate fitting agent for FAW-EV path tracking controller [38]. The sequence is discretely described using the following z-transformed expression.

$$\begin{aligned} \Gamma_1(z) &= \frac{\sqrt{1-a^2}}{1-az^{-1}} \\ \Gamma_2(z) &= \frac{\sqrt{1-a^2}}{1-az^{-1}}\frac{z^{-1}-a}{1-az^{-1}} \\ &\vdots \\ \Gamma_{N_L}(z) &= \frac{\sqrt{1-a^2}}{1-az^{-1}}\left(\frac{z^{-1}-a}{1-az^{-1}}\right)^{N_L-1} \end{aligned} \tag{12}$$

where a and N_L denote the scale factor and term number, respectively, of the discrete-time Laguerre function sequence, which possesses orthogonality as

$$\begin{cases} \frac{1}{2\pi}\int_{-\pi}^{\pi} \Gamma_m(e^{j\omega})\Gamma_m(e^{j\omega})d\omega = 1\ , \ m = n \\ \frac{1}{2\pi}\int_{-\pi}^{\pi} \Gamma_m(e^{j\omega})d\omega\Gamma_n(e^{j\omega}) = 0\ , \ m \ne n \end{cases} \tag{13}$$

Since the inverse z-transform of the Laguerre function does not become more concise, the discrete-time Laguerre function sequence is simply expressed in vector form as

$$L(i) = [l_1(i)\ l_2(i) \cdots\ l_{N_L}(i)]^T \tag{14}$$

where $l_i(k)$ represents the inverse z-transform of $\Gamma_k(z,a)$, whose difference equation can be described as

$$\Gamma_k(z) = \Gamma_{k-1}(z)\frac{z^{-1}-a}{1-az^{-1}}\ k = 1, 2, \cdots N_L \tag{15}$$

Thus, the inverse z-transform discrete-time Laguerre function sequence satisfies the difference equation as

$$L(k+1) = A_l L(k) \tag{16}$$

with

$$A_{l(N_L\times N_L)} = \begin{bmatrix} a & 0 & 0 & \cdots & 0 \\ \beta & a & 0 & \cdots & 0 \\ -a\beta & \beta & a & \cdots & 0 \\ \vdots & \vdots & \ddots & \ddots & \vdots \\ (-1)^{N_L-2}a^{N_L-2}\beta & (-1)^{N_L-3}a^{N_L-3}\beta & \cdots & \beta & a \end{bmatrix}$$

where $\beta = (1-a^2)$. Since a system $H(i)$ can be fit as

$$H(i) = c_1 l_1(i) + c_2 l_2(i) + \cdots + c_{N_L} l_{N_L}(i) \tag{17}$$

the control input increment at an arbitrary future time step within the control horizon can be represented as

$$\Delta u(k+i) = L(i)^T \eta = \sum_{j=1}^{N_L} c_j(k) l_j(i),\ i = 0, 2, \cdots N_c \tag{18}$$

where $\eta = [c_1\ c_2 \cdots c_{N_L}]^T$ and c_j is the fitting coefficient. Therefore, (8) can be approximately transformed as

$$Y_{sys}(k) = \Psi_k \xi(k\,|\,t) + \Theta_k K_L \eta \tag{19}$$

where the augmented matrix

$$K_{L(N_c\times N_L)} = \begin{bmatrix} L(0)^T \\ L(1)^T \\ \vdots \\ L(N_c-1)^T \end{bmatrix} \tag{20}$$

With the orthogonality described with (13), the QP problem (10) can be simply rewritten as

$$\min \quad J_L = V_L^T H_L V_L + G_L V_L \tag{21a}$$

$$s.t. \quad \Delta\tilde{U}_{min} \le K_L \eta \le \Delta\tilde{U}_{max} \tag{21b}$$

where the vector of optimization control parameter is changed into $V_L = [\eta, \varepsilon]$, in which the dimension of η is N_L.

The coefficient matrices of (21) are arranged as

$$H_L = \begin{bmatrix} K_L \Theta_k^T Q\, \Theta_k K_L^T & 0 \\ 0 & \rho \end{bmatrix} \quad G_L = \begin{bmatrix} 2E_k^T Q\, \Theta_k K_L^T & 0 \end{bmatrix} \tag{22}$$

Paper [26] gives the stability proof of the MPC with Laguerre function, and the control input increment at the current time can be achieved by

$$\Delta u(k\,|t\,) = L(0)^T \eta \tag{23}$$

Remark 1: The scale factor a is closely related to the term number that is primarily required to fit $\Delta U(k)$. While $a = 0$, traditional MPC path tracking performance can be uniformly realized by setting N_L equal to N_c [38]. For reducing the dimension of V_L, we set $0 < a < 1$; therefore, the similar path tracking control performance can be achieved with the optimization control parameter dimension of $N_L + 1$, which is far less than $N_c + 1$ within traditional MPC of (10). This advantage reduces the computational complexity without sacrificing the path tracking control performance.

C. SOLVING MATHEMATICAL PROBLEM WITH EXPONENTIAL WEIGHT

Actually, the mathematical problem is inherent in MPC technology. The first derivative of the cost function J_L described in (21a) is achieved by

$$\frac{\partial J_L}{\partial V_L} = 2H_L V_L + G_L \tag{24}$$

Without considering constraints, the equation

$$\frac{\partial J_L}{\partial V_L} = 0 \tag{25}$$

is necessary for minimizing J_L; thus, the optimal solution is

$$V_L = -H_L^{-1} G_L \Big/ 2 \tag{26}$$

with the assumption of existing H_L^{-1}, which is called the Hessian matrix of the MPC algorithm.

When predicting future system outputs within (21a), we set the convolution sum matrix $\phi = \Theta_k K_L$, and the difference relationship between the convolution matrix elements is

$$\phi(m) = \begin{cases} \tilde{A}_{k,t}\phi(m-1) + \phi(1)(A_l^{m-1})^T, 0 \le m < N_c \\ \tilde{A}_{k,t}\phi(m-1) \quad , N_c \le m \le N_p \end{cases} \tag{27}$$

Because of the integral action in the MPC framework, norms of the matrix powers $\left\|\tilde{A}_{k,t}^m\right\|$ and $\|\phi\|$ do not decay to zero as N_p increases; thus, the Hessian matrix H_L^{-1} possesses a large magnitude. For vehicle path tracking control based on MPC, a long N_p is always chosen to ensure vehicle dynamic stability during severe driving conditions, but the large magnitude of H_L^{-1} accumulates strongly to the instability of the predictive plant and thereby leads to system ill-conditioning, resulting in high sensitivity to even slight disturbances [39], [40].

The condition number, a quantization index for system ill-conditioning, can be computed by

$$\gamma_c(H_L) = \left|\lambda_{max}(H_L)\right| \Big/ \left|\lambda_{min}(H_L)\right| \tag{28}$$

where $\lambda_{max}(H_L)$ and $\lambda_{min}(H_L)$ are maximal and minimal characteristic values, respectively. γ_c can be considered a magnified degree of the unexpected sensitivity caused by the ill-conditioning. As N_p elongates, $\gamma_c(H_L^{-1})$ dramatically increases to a value that is far greater than "1" and tends to infinity. This large value represents a high level of numerical sensitivity to disturbances and consequently reduces the robustness of the path tracking control system.

To address this issue, the exponential weight α^{-2j} with decreasing characteristic is introduced to the cost function of the MPC path tracking controller. The introduction of α^{-2j} aims to restore a stability margin by placing less weighting on future tracking errors and control input increments, and the cost functions (9a) can be changed to

$$J = \sum_{i=1}^{N_p} \alpha^{-2i} \left\| y_{ref}(k+i\,|k\,) - y(k+i\,|k\,) \right\|_Q^2 + \sum_{i=0}^{Nc-1} \alpha^{-2i} \left\| \Delta u(k+i|\,k) \right\|_R^2 + \rho\, \varepsilon^2 \tag{29}$$

Both $\lambda_{max}(H_L)$ and $\lambda_{min}(H_L)$ can be converged into a bounded region, significantly reducing the condition number and therefore ameliorating the ill-conditioning of the path tracking system with MPC, and paper [27] gives the feasibility proof of the exponential weight introduction.

Actually, the exponential weighted cost function acts through the transformed control input increments and state variables instead of cost function design; consequently, ΔU and ξ change to

$$\Delta \hat{U} = [\Delta\hat{u}(k)\ \Delta\hat{u}(k+1)\ \Delta\hat{u}(k+2) \cdots \Delta\hat{u}(k+N_c-1)]^T$$

and

$$\hat{\xi} = [\hat{\xi}(k+1)^T\ \hat{\xi}(k+2)^T \cdots \hat{\xi}(k+N_p)^T]^T$$

where

$$\Delta\hat{u}(k+i) = \alpha^{-i}\Delta u(k+i)^T \ = \alpha^{-i} L(i)^T \eta$$
$$\hat{\xi}(k+i) = \alpha^{-i}\xi(k+i)^T$$

This transformation is achieved by changing the predictive plant in (7) to

$$\hat{\xi}(k+1\,|t\,) = \hat{A}_{k,t}\hat{\xi}(k) + \hat{B}_{k,t}\Delta\hat{u}(k) \tag{30}$$

with

$$\hat{A}_{k,t} = \tilde{A}_{k,t} \Big/ \alpha,\ \hat{B}_{k,t} = \tilde{B}_{k,t} \Big/ \alpha \tag{31}$$

In summary, the LEMPC path tracking control can be formulated as an optimization control problem as

$$min\ \hat{J}_L = V_L^T \hat{H}_L V_L + \hat{G}_L V_L \tag{32a}$$
$$s.t.\ \Delta\tilde{U}_{min} \le \Lambda K_L \eta \le \Delta\tilde{U}_{max} \tag{32b}$$

where $\hat{H}_L$ and $\hat{G}_L$ are achieved by introducing (31) into (7) and (22), respectively. The transformation matrix in (32b) is defined as

$$\Lambda = \begin{bmatrix} I & 0 & \cdots & 0 \\ 0 & \alpha^1 I & \cdots & 0 \\ \vdots & \vdots & \ddots & \vdots \\ 0 & 0 & \cdots & \alpha^{N_c-1} I \end{bmatrix} \tag{33}$$

Remark 2: To ensure closed-loop stability, α should be chosen to be slightly larger than "1".

The current control input of the LEMPC path tracking controller can be achieved by (11), with the current control input increment computed by (23).

D. PARAMETERIZATION ILLUSTRATION

Actually, the path tracking controller should adjust its performance to the variable driving condition. For the MPC path tracking controller with a basic framework, the value of N_c significantly affects the control performance, such as the tracking accuracy. The influence of N_p also cannot be ignored. For example, an MPC path tracking controller with long N_p controls the vehicle with greater stability; however, tracking accuracy is sacrificed. In contrast, a controller with short N_p often encounters challenges in ensuring dynamic stability during severe driving conditions.

Unfortunately for the path tracking controller based on the traditional MPC, it is challenging to finely adjust the control performance because N_c and N_p must be integers. Moreover, in addition to the severe system ill-conditioning, the system ill-condition gap between different N_p is very large. These mathematical problems lead to violent fluctuation in the control input during N_p adjustment, therefore largely reducing the path tracking control performances of both the tracking accuracy and vehicle dynamic stability.

Within the LEMPC path tracking controller, the parameterization ability is mainly summarized as follows:

First, the Laguerre function possesses an attenuating property whose extent depends on the value of the scale factor a. Such a Laguerre function with larger a needs more sample points to decay to 0 [26]. The difference of the attenuating property determined by a becomes the key to finely regulate the control performance of the LEMPC path tracking controller.

Second, the system ill-conditioning is largely improved by introducing the exponential weight α^{-2j}; the system ill-condition gap between different N_p values can also be reduced considerably, so the N_p can be adjusted online to different driving conditions without large fluctuation.

The regulation principles are illustrated through several simulations in part C of Section IV

E. MOTION REALIZATION FOR FAW-EV

As the foundation of actualizing path tracking, a motion realization method with FAW-EV was presented and studied in our previous paper [41]. To aid in understanding, the motion realization process is illustrated briefly here.

The path tracking motion with FAW-EV is realized by a hierarchical structure that is functionally divided into three tasks: desired motion computation, tire force distribution, and actuator implementation.

The desired motion computation transforms the desired front steering angle and desired vehicle velocities to total vehicle efforts, which includes F_{xd}, F_{yd}, and M_{zd}. For stability, the desired lateral vehicle velocity V_{yd} is set as 0. With the desired longitudinal velocity V_{xd} preset and the desired front steering angle δ_{fd} achieved by the LEMPC path tracking controller, the desired motions are defined as

$$\begin{cases} \dot{\psi}_d = \left(V_x / \left(l_f + l_r\right)\right) \cdot \delta_{fd} / \left(1 + K_g V_x^2\right) \\ V_{xd} = V_{xd} \\ V_{yd} = 0 \end{cases} \tag{34}$$

where K_g is the understeering degree. For decoupling the nonlinear relationship between motions on those three directions, SMC technology is employed to achieve the desired total efforts as (35), as shown at the bottom of this page. In addition, p_3 and q_3 denote positive odd numbers, and $1 < p_3/q_3 < 2$, s_1, s_2, and s_3 are the sliding mode surfaces defined as minimizing differences away from desired motions on those three directions, and the function *sat* is defined as

$$sat\left(\frac{s_k}{\phi_k}\right) = \begin{cases} s_k/\phi_k, if \ |s_k| < \phi_k \\ sgn\left(s_k/\phi_k\right), if \ |s_k| \geq \phi_k \end{cases} \tag{36}$$

For the tire force distribution, the desired total efforts achieved by (35) are divided into eight tire forces by solving

$$F_{xd} = m\left(-V_y\dot{\psi} + \dot{V}_{xd} - \eta_{1n} sat\left(s_1/\phi_1\right)\right), \{F_{xd} \,|F_{xd}| \leq \mu mg\} \tag{35a}$$

$$F_{yd} = m\left(V_x\dot{\psi} - \eta_{2n} sat\left(s_2/\phi_2\right)\right), \left\{F_{yd} \,\middle|\, |F_{yd}| \leq \mu mg\right\} \tag{35b}$$

$$\begin{aligned} M_{zd} = I_z \Bigg(& \left(a_x + V_y\dot{\psi}\right)\left(\frac{\delta_{fd}/\left(l_f + l_r\right)}{1 + K_g V_x^2} - \frac{2K_g V_x^2 \delta_{fd}/\left(l_f + l_r\right)}{\left(1 + K_g V_x^2\right)^2}\right) \\ & + \frac{V_x \dot{\delta}_{fd}/\left(l_f + l_r\right)}{1 + K_g V_x^2} + \frac{\alpha_3 q_3}{\beta_3 p_3}\left(\dot{\psi} - \dot{\psi}_d\right)^{2 - p_3/q_3}\left(\frac{-\alpha_{3n} s_3 - \beta_{3n} s_3^{q_{3n}/p_{3n}}}{\alpha_3\left(\dot{\psi} - \dot{\psi}_d\right)} - 1\right)\Bigg) \end{aligned} \tag{35c}$$

the following QP problem:

$$min\ J_{CA} = \sum_{i=l}^{r}\sum_{j=f}^{r}\frac{X_{w\_ij}^2 + Y_{w\_ij}^2}{\mu_{ij}^2 F_{z\_ij}^2} \tag{37a}$$

$$s.t.\ A_{eq}u_{CA} = b_{eq} \tag{37b}$$

$$A_{lim}u_{CA} \le b_{lim} \tag{37c}$$

where the vector of optimization control parameters is defined as

$$u_{CA} = \left[X_{w\_lf}\ X_{w\_rf}\ X_{w\_lr}\ X_{w\_rr}\ Y_{w\_lf}\ Y_{w\_rf}\ Y_{w\_lr}\ Y_{w\_rr}\right]^T$$

which consists of eight tire forces as shown in Fig. 4. (37a) is the cost function defined as the sum of the tire workloads to maximize the stable margin. According to the relationships between the tire forces and total efforts described by (3), the equivalent constraints are introduced as (37b). To ensure tire stability, the linearized tire stability limit is introduced as (37c), corresponding to

$$\begin{aligned} -\mu_{ij}F_{z\_ij} &< X_{w\_ij} < \mu_{ij}F_{z\_ij}, \\ -\mu_{ij}F_{z\_ij} &< Y_{w\_ij} < \mu_{ij}F_{z\_ij}, \\ -\sqrt{2}\mu_{ij}F_{z\_ij} &< X_{w\_ij} + Y_{w\_ij} < \sqrt{2}\mu_{ij}F_{z\_ij}, \\ -\sqrt{2}\mu_{ij}F_{z\_ij} &< Y_{w\_ij} - X_{w\_ij} < \sqrt{2}\mu_{ij}F_{z\_ij} \end{aligned} \tag{38}$$

Actuator implementation translates the tire forces to wheel driving torques and steering angles, which can be directly realized by the actuators. First, $\delta_{ij} \approx \sigma_{ij}$ is assumed according to the infinitesimal sideslip angle; with (4), it can be obtained that

$$\begin{cases} F_{y\_ij} \approx -X_{w\_ij}\sin\sigma_{ij} + Y_{w\_ij}\cos\sigma_{ij} \\ F_{x\_ij}^* = X_{w\_ij}\cos\sigma_{ij} + Y_{w\_ij}\sin\sigma_{ij} \end{cases} \tag{39}$$

where $F_{x\_ij}^*$ denotes the estimated longitudinal tire force. With the inversion of the tire model as (5), the sideslip angle of the tire can be computed by

$$\alpha_{ij} = -\frac{\mu_{ij}}{k_{ij}}\tan\left(\frac{k_{ij}}{\mu_{ij}}\cdot\frac{F_{y\_ij}}{C_{\alpha\_ij}\sqrt{1-\left(\frac{F_{x\_ij}^*\cos 22.5^\circ}{\mu_{ij}F_{z\_ij}}\right)^2}}\right) \tag{40}$$

The wheel steering angle is computed by

$$\delta_{ij} = \sigma_{ij} - \alpha_{ij} \tag{41}$$

with σ_{ij} achieved by (6). The wheel driving torque is computed by

$$T_{w\_ij} = J_{w\_ij}\dot{\omega}_{ij} + F_{x\_ij}R_{w\_ij} + T_{b\_ij} \tag{42}$$

where $\dot{\omega}_{ij}$, R_{w_ij}, T_{b_ij} and J_{w_ij} denote the wheel rotation rate, effective rolling radius, friction braking torque and wheel rolling inertia, respectively. The longitudinal tire force F_{x_ij} is computed according to equation (4).

IV. SIMULATION RESULTS AND ILLUSTRATION

The simulations are carried out using the software of Simulink combined with Carsim, in which a high-fidelity model of the FAW-EV is built. The major simulation parameters are listed in Table 1. The FAW-EV is controlled to track a double-change lane (DLC), with the desired outputs defined by

$$\begin{aligned} Y_{ref}(X) &= \frac{d_{y1}}{2}(1+\tanh(z_1)) - \frac{d_{y2}}{2}(1+\tanh(z_2)) \\ \psi_{ref}(X) &= tan^{-1}(d_{y1}(\frac{1}{\cosh(z_1)})^2(\frac{1.2}{d_{x1}}) \\ &\quad - d_{y2}(\frac{1}{\cosh(z_1)})^2(\frac{1.2}{d_{x2}})) \end{aligned} \tag{43}$$

TABLE 1. Simulation parameters.

Symbol	Interpretation	Value (Unit)
m	total mass	1723 (kg)
I_z	moment of inertia	4175 $(kg\cdot m^2)$
l_f	front axle distance	1.232 (m)
l_r	rear axle distance	1.468 (m)
C_{cf}	front cornering stiffness	62900 (N/rad)
C_{cr}	rear cornering stiffness	62700 (N/rad)
T	model discretized step	0.02 (s)

where

$$\begin{aligned} z_1 &= 2.4(X-27.19)/25 - 1.2 \\ z_2 &= 2.4(X-56.46)/21.95 - 1.2 \end{aligned}$$

and d_{x1}, d_{x2}, d_{y1}, and d_{y2} are set as 25, 21.59, 4.05, and 5.7, respectively. The reason for choosing the DLC as the reference lane is that the multiple-curvature characteristic of it can feature different driving conditions by combing with different vehicle velocities and road conditions.

The initial values for the QP problems of (32) and (37) are set as zero in this paper, and the Matlab function of ''quadprog'' is used to solving the QP problems. The simulation verification is mainly divided into three parts: first, control performance and advantage of MPC path tracking controller with the incorporated Laguerre function are interpreted and verified in part A, and then part B proves the availability for improving the path tracking control robustness by solving the mathematical problem with introduction of exponential weight. Finally, the parameterization ability and main adjusted ideas for path tracking control with LEMPC are interpreted by combining with several simulation results in part C.

A. INTRODUCTION OF THE LAGUERRE FUNCTION

For ensuring the close-loop stability and to consider practical feasibility, we set a long N_p as 36. With the constant friction factor μ_{ij} as 0.75, the simulations with different longitudinal velocities of 15 m/s and 30 m/s are implemented.

Set the term number N_L as 4 and scale factor a as 0.9; the N_c of MPC introduced Laguerre function (LMPC) is set as 36.

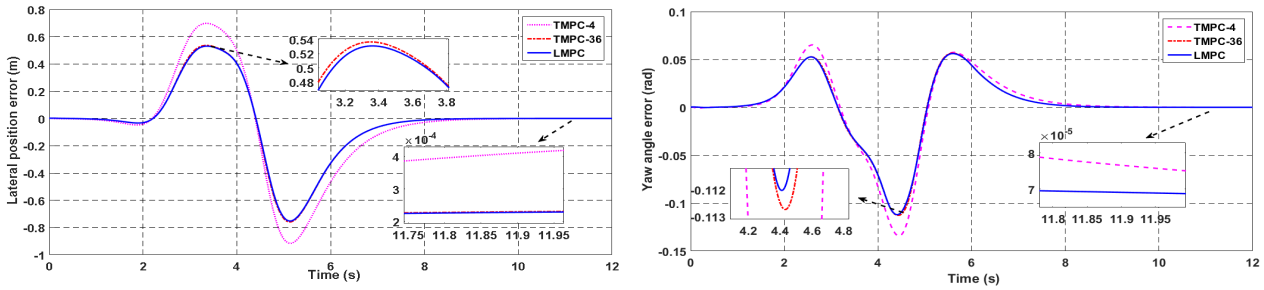

FIGURE 6. Path tracking errors for $V_{xd} = 15\ m/s$, $\mu_{ij} = 0.75$. (a) Lateral position tracking error (b) Yaw angle tracking error.

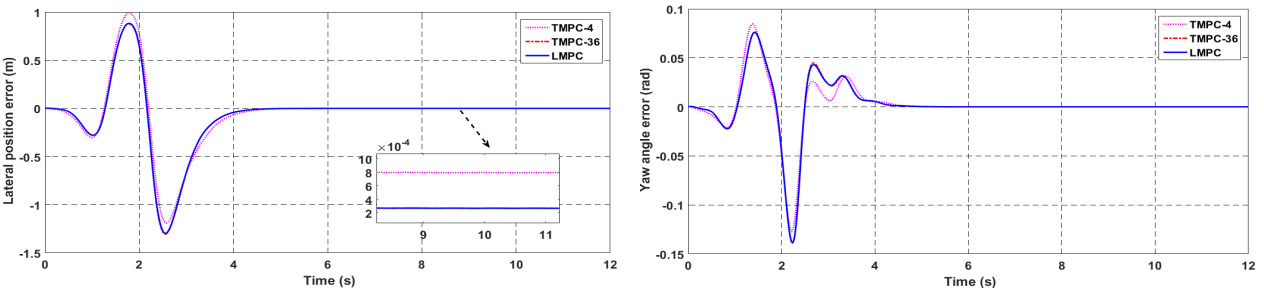

FIGURE 7. Path tracking errors for $V_{xd} = 30\ m/s$, $\mu_{ij} = 0.75$. (a) Lateral position tracking error. (b) Yaw angle tracking error.

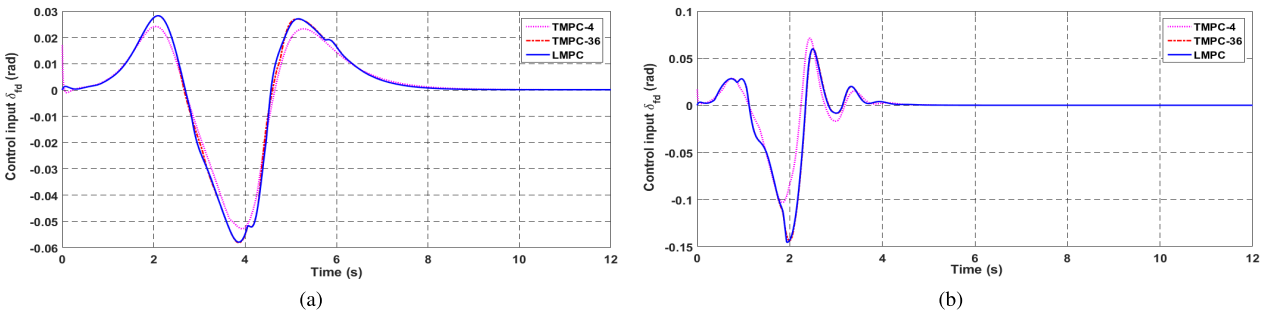

FIGURE 8. Path tracking control inputs. (a) $V_{xd} = 15\ m/s$, $\mu_{ij} = 0.75$. (b) $V_{xd} = 30\ m/s$, $\mu_{ij} = 0.75$.

For outstanding performance of the proposed path tracking controller, the traditional MPC controllers with control horizon length of 4 (TMPC-4) and 36 (TMPC-36) are introduced as comparisons. The results are shown in Fig. 6 to Fig. 8. For in-depth researching of the tracking performance of different controllers, an index that quantifies the tracking performance is given as

$$Q_{track\_i} = \sqrt{\frac{\sum_{j=1}^{t_{sim}/T_q} \left(y_{ref}(j) - y_{sys}(j)\right)^2}{t_{sim}/T_q - 1}},\ \forall i \in \{\psi, Y\} \qquad (44)$$

where t_{sim} is the simulation duration time and T_q is the controller sampling step. The tracking performance indexes of simulations for the three controllers are given in Table 2 and Table 3, in which the dimension of the optimization control parameter matrix V or V_L is denoted as n.

Fig. 6 and part of the Fig. 7 show that vehicles controlled by the two MPC controllers with long N_c (LMPC and TMPC-36) possess higher path tracking accuracy than that controlled by the traditional MPC controller with short N_c (TMPC-4). Notably, Fig. 7 shows a lower tracking accuracy of LMPC and TMPC-36 during simulation duration from 2nd to 4th second. Fig. 8(b) indicates the reason that the radical control motions used to achieve high tracking accuracy reach the constraint boundary during severe driving conditions. Such control saturation leads to unexpected control performances [40], which influences the tracking index in Table 3 but can be mitigated by adjustment of the Laguerre function parameters. Additionally, the large tracking error mostly influenced by the long prediction horizon can be shrank by adjusting N_p, which is illustrated in the last part of this section.

Discarding the control saturation, the higher tracking accuracy can be achieved by controllers with a long

TABLE 2. Indexes for condition of $V_{xd} = 15\ m/s$, $\mu_{ij} = 0.75$.

Controller	LEMPC	TMPC-36	TMPC-4
n	4+1	36+1	4+1
Q_{track_Y}	0.2676	0.2704	0.3421
Q_{track_ψ}	0.0339	0.0343	0.0396

TABLE 3. Indexes for the condition of $V_{xd} = 30\ m/s$, $\mu_{ij} = 0.75$.

Controller	LEMPC	TMPC-36	TMPC-4
n	4+1	36+1	4+1
Q_{track_Y}	0.3310	0.3317	0.3311
Q_{track_ψ}	0.0261	0.0262	0.0264

control horizon. Notably, Table 2 and Table 3 indicate that relative to TMPC-36, the LMPC path tracking controller can realize similar path tracking control performance with only 5 (computed by $N_L + 1$) optimization control parameters, which is far less than that of TMPC-36 (with an optimization control parameter quantity of 37 computed by $N_c + 1$). This result indicates that the proposed MPC controller with an incorporated Laguerre function can substantially reduce the computational complexity.

Moreover, it is observed that the LMPC can control the vehicle to track the reference path with more accuracy than that controlled by TMPC-36. The reason is because as N_L increases, the control trajectory of LEMPC can be converged to an underlying trajectory instead of the control trajectory of the traditional MPC; this trajectory is interpreted in the last part of this section.

B. MATHEMATICAL PROBLEM IMPROVEMENT WITH EXPONENTIAL WEIGHT

For the MPC path tracking controller, the robustness deterioration by mathematical problems is closely related to N_p, so this part sets the driving condition of the middle desired longitudinal velocity ($V_{xd} = 17\ m/s$) and friction factor ($\mu_{ij} = 0.5$), and the control performance of MPC controller with Laguerre function and exponential weight (LEMPC) is compared with that of the controller without exponential weight (LMPC).

Since the mathematical problem becomes severe along with N_p elongating, first, for quantifying the ability to solve the mathematical problem, we vary N_p to increase from 20 to 36, and the curves of condition number are shown in Fig. 9.

It is observed that the condition number is significantly reduced by the proposed method (with 95.11% reduction at $N_p = 36$), which means that the ill-conditioning has been largely ameliorated with LEMPC.

Then, for further proving the path tracking robustness improvement according to the relationship between N_p and the tracking system ill-conditioning, two sets of simulations with N_p set to constants of 25 and 30 are implemented, and the

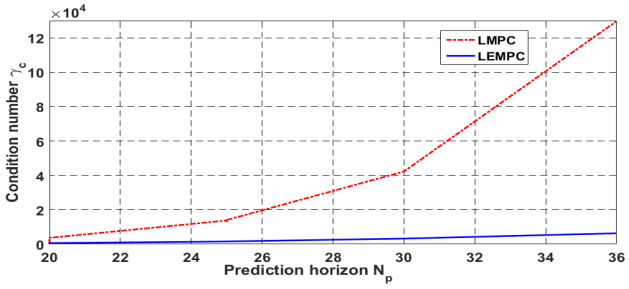

FIGURE 9. Condition number of different prediction horizons.

disturbances with different amplitudes are typically imposed to yaw angle signal at different simulation times (3 ψ at the 3rd second and 50 ψ at the 10th second). The results are shown as Fig. 10 to Fig. 12.

Fig. 12 comparably shows that for LMPC with a longer prediction horizon, the control input influence caused by disturbances is much more severe than that with shorter N_p. This finding illustrates the incremental progression of system ill-conditioning as N_p elongates, which conforms to the results shown in Fig. 9. The large scale of vibration of the control input indicates high sensitivity and weak robustness of LMPC to the disturbance.

Relative to LMPC, it can be found in Fig. 10 and Fig. 11 that with two prediction horizon lengths, the LEMPC path tracking controller with exponential weight possesses stronger robustness, which is embodied mainly in the slighter shake caused by the disturbance and in a faster return to the stable state.

Additionally, with the two prediction horizon lengths, the introduction of exponential weight can improve the robustness without sacrificing tracking accuracy.

C. PARAMETERIZATION ABILITY FOR ONLINE ADAPTION

An important advantage of the proposed method is the parameterization of the LEMPC path tracking controller, which provides access for fine online adjustment of the control performance to driving conditions with different dynamic and path tracking requirements. The parameterized variables are the Laguerre function parameters (N_L, a) and prediction horizon N_p.

First, we set different longitudinal velocities and friction factors; with the reference path aforementioned, several simulations are implemented with different N_L and a. Part A of this section indicates that the constraints dynamically affect the control motion; for studying the influence of Laguerre function parameters without confusion, the constraints are ignored, and the results are shown as Fig. 13 to Fig. 15, with the curve label form of "$N_L - a$".

Fig. 13 shows that with the same value of N_L, a larger a is associated with a higher tracking accuracy. Fig. 14 indicates, however, that for the FAW-EV path tracking during severe conditions, the LEMPC path tracking controller with larger a leads to a radical control input of the desired front steering

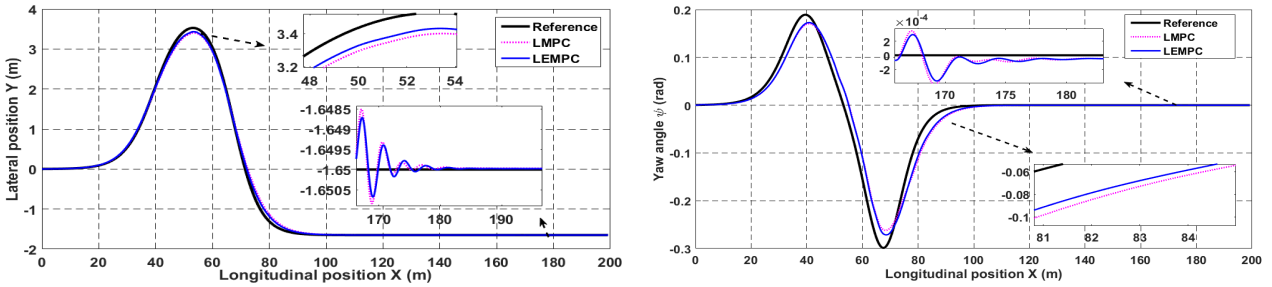

(a) (b)

FIGURE 10. Path tracking control performance for $N_p = 25$, $V_{xd} = 17\ m/s$, $\mu_{ij} = 0.5$, with introduced disturbances. (a) Lateral position tracking. (b) Yaw angle tracking.

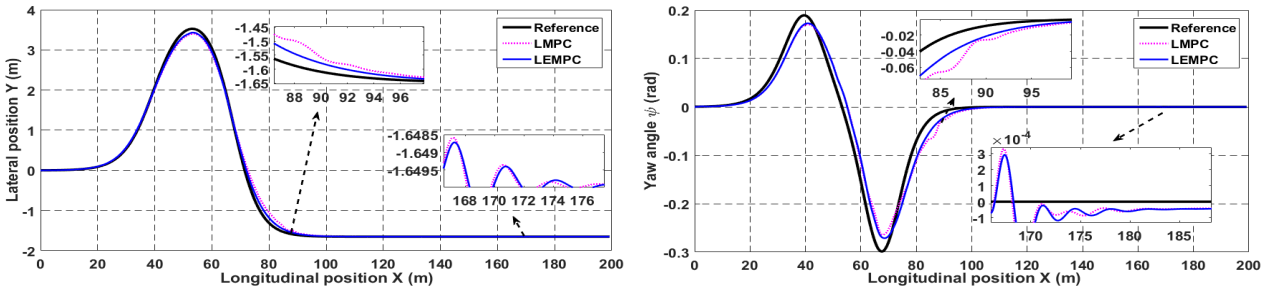

(a) (b)

FIGURE 11. Path tracking control performance for $N_p = 30$, $V_{xd} = 17\ m/s$, $\mu_{ij} = 0.5$, with introduced disturbances. (a) Lateral position tracking. (b) Yaw angle tracking.

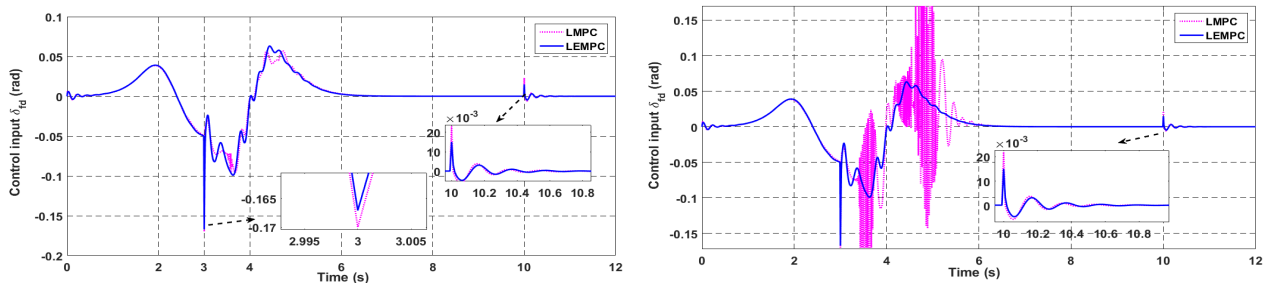

(a) (b)

FIGURE 12. Path tracking control inputs with introduced disturbances. (a) Control inputs for $N_p = 25$. (b) Control inputs for $N_p = 30$.

angle, which produces a very dangerous large yaw overshoot. Therefore, online adjustment of a to different driving conditions is recommended for maximizing the control advantage of the LEMPC path tracking controller.

Additionally, Fig. 15 shows that with the constant scale factor a, as N_L increases, the control performance converges to an underlying trajectory that is uniquely decided by the DLQR as soon as Q and R are identified; this is the reason for the higher tracking accuracy with LMPC than that with TMPC-36 as discussed in part A of this section. Fig. 13 and Fig. 15 indicate that with large N_L, adjustment of a cannot efficiently affect the path tracking control performance.

As discussed above, for realizing online adapting control performance to the varied driving conditions, a regulated principle for Laguerre parameters is simply given as follows: set a low term number ($N_L \leq 4$); therefore the scale factor a can be regarded as a fine-tuning knob, which can be adjusted online to the current dynamic stability and tracking accuracy requirements.

Then, it can be found in Fig. 9 that both the condition number and the condition number gaps between different N_p are significantly reduced by LEMPC. Considering constant Laguerre parameters ($a = 0.9, N_L = 2$), switching N_p at the 3rd second; the control inputs and control input increments of LEMPC and traditional MPC are shown as Fig. 16. It shows that the fluctuation of control input during switching N_p can be largely reduced by employing LEMPC.

For illustrating the impact of N_p on LEMPC path tracking control performance, set a severe driving condition ($V_{xd} = 20\ m/s, \mu_{ij} = 0.4$), the compared results of controllers with

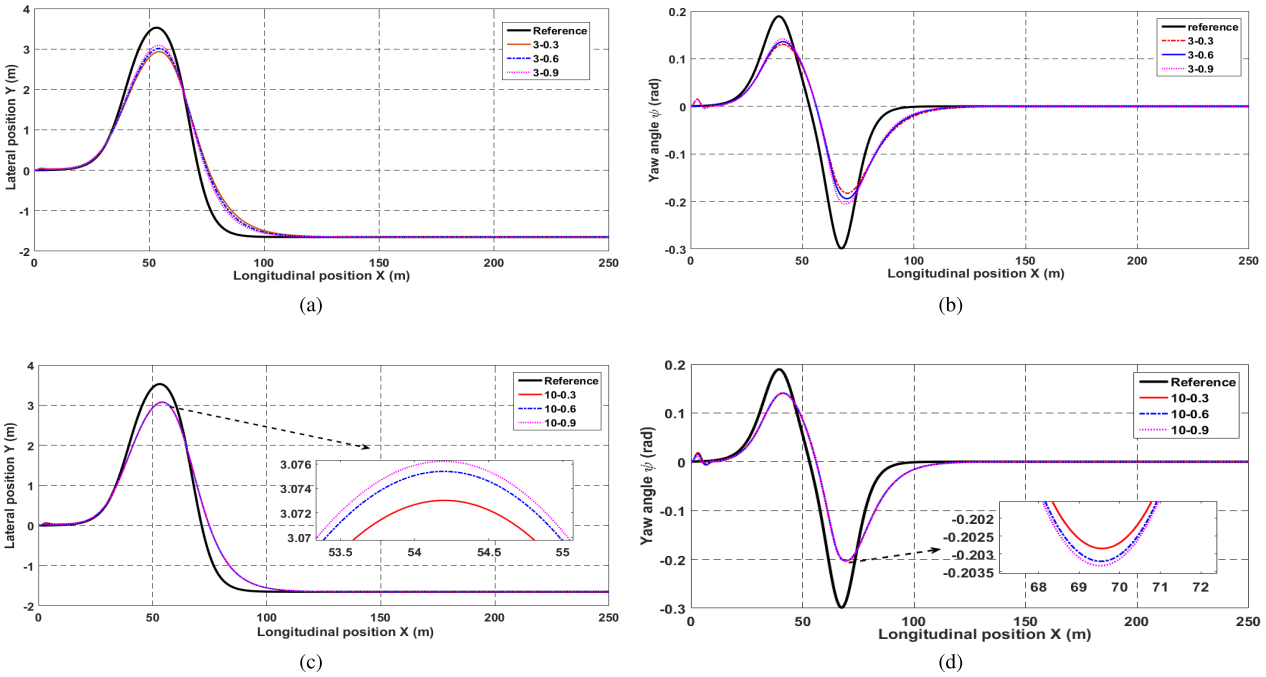

FIGURE 13. Path tracking control performances for different N_L and a under conditions of $V_{xd} = 15\ m/s$, $\mu_{ij} = 0.5$. (a) Lateral position tracking. (b) Yaw angle tracking. (c) Lateral position tracking. (d) Yaw angle tracking.

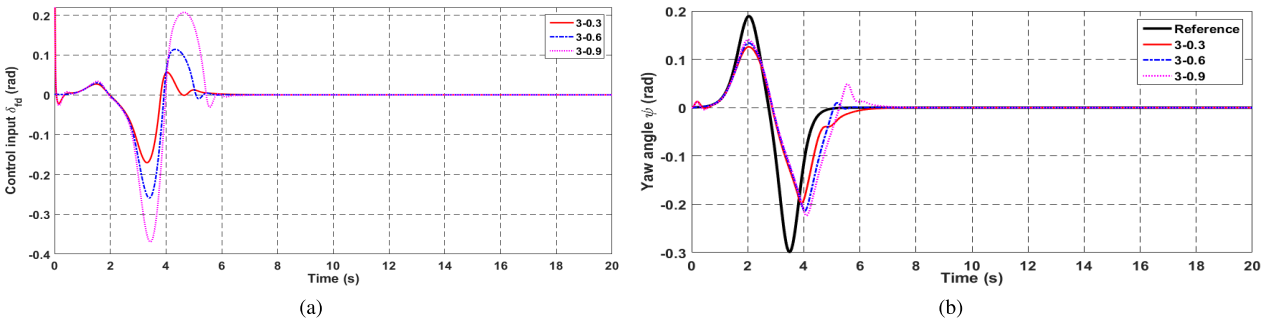

FIGURE 14. Path tracking control performances for different a under severe conditions of $V_{xd} = 22\ m/s$, $\mu_{ij} = 0.3$. (a) Control inputs of path tracking controllers. (b) Yaw angle tracking.

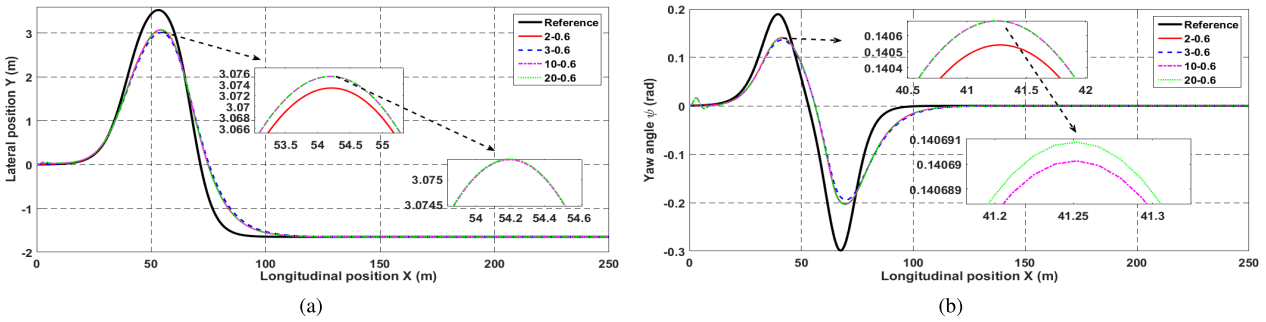

FIGURE 15. Path tracking control performances for different N_L under conditions of $V_{xd} = 15\ m/s$, $\mu_{ij} = 0.5$. (a) Lateral position tracking. (b) Yaw angle tracking.

different prediction horizon settings are shown in Fig.17, in which the LEMPC controllers both with fixed N_p of 20 and 36 are set as the comparisons to highlight the advantage of controller with varied N_p. It can be found that vehicle manoeuvred by controller with fixed short N_p experiences serious dynamic unstability during severe driving condition;

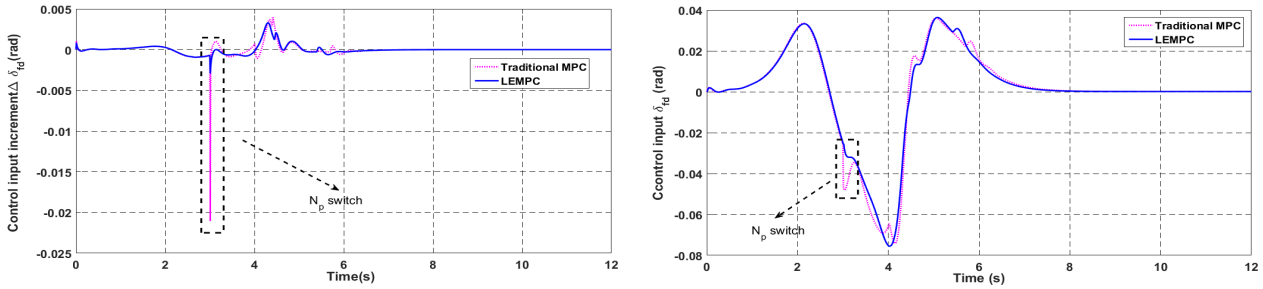

(a) (b)

FIGURE 16. Control input of the path tracking controller during switching N_p. (a) Control input increments of the path tracking controllers. (b) Control inputs of the path tracking controllers.

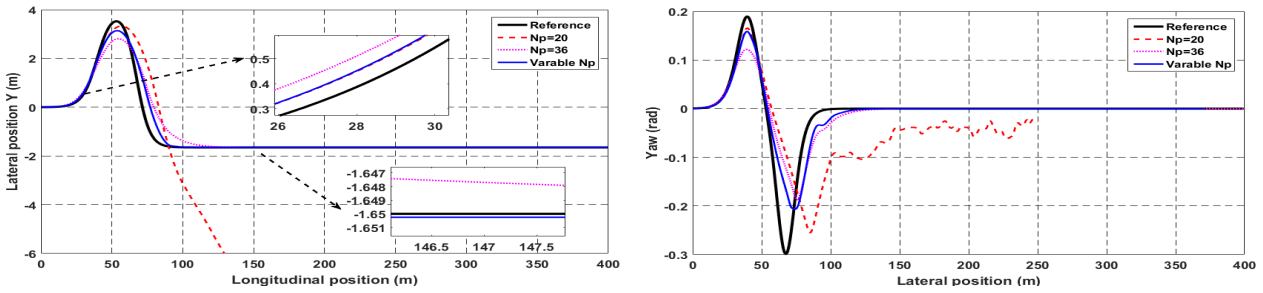

(a) (b)

FIGURE 17. Path tracking control performances for different N_p settings. (a) Lateral position tracking. (b) Yaw angle tracking.

controller with fixed long N_p can ensure the dynamic stability of the vehicle, but during dynamic stable driving conditions, the tracking accuracy makes concession for the conservative dynamic stability; for controller with variable N_p, the relatively high tracking accuracy is ensured by online choosing a short N_p, which is elongated online to a long length to enlarge stable margin only during dynamic unstable conditions, therefore the vehicle dynamic stability can also be guaranteed.

In the last simulation, the N_p is online adjusted at given simulation times, actually, which should be adjusted according to current or predicted future vehicle states and control requirements. The advanced adjustment method should be studied in future work, and the main idea can be summarized as follows: First, build the stability boundary in the stability phase plane, and judge whether the current or future vehicle dynamic stability exceeds dynamic stable region. Then, if the vehicle be manoeuvred within the dynamic stable region, the prediction horizon can be set as a minimum value; otherwise, the prediction horizon should be online adjusted to a relative long length to ensure the vehicle dynamic stability.

V. CONCLUSION AND FUTURE WORK

An improved path tracking controller based on LEMPC for a FAW-EV is proposed. A parsimonious description for the future control input increment trajectory is achieved by Laguerre function fitting, and an exponential weight is introduced to solve the mathematical problem inherent in the MPC path tracking controller. The proposed method significantly reduces the computational complexity without sacrificing path tracking control performance (the dimension of the optimization control parameter matrix is reduced from 37 to 5), and the robustness of FAW-EV path tracking control system is enhanced by solving the mathematical problem (with 95.11% reduction of ill-conditioning at $N_p = 36$). Moreover, the proposed method provides parameterization, which is key to adjust the path tracking control performance online for diverse driving conditions.

The main idea for adjusting parameters of LEMPC path tracking controller in this paper is only a preliminary work. For fully taking advantage of the adjustability of the LEMPC path tracking controller, the relation between the vehicle performances (such as tracking accuracy and dynamic stability) and parameters of LEMPC (N_L, a, and N_p) should be finely quantized, and a more refined online-regulated method for adaptive path tracking control should be developed in future work.

REFERENCES

[1] H. N. de Melo, J. P. F. Trovão, P. G. Pereirinha, H. M. Jorge, and C. H. Antunes, "A controllable bidirectional battery charger for electric vehicles with vehicle-to-grid capability," *IEEE Trans. Veh. Technol.*, vol. 67, no. 1, pp. 114–123, Jan. 2017.

[2] B. Li, H. Du, and W. Li, "A potential field approach-based trajectory control for autonomous electric vehicles with in-wheel motors," *IEEE Trans. Intell. Transp.*, vol. 18, no. 8, pp. 2044–2055, Aug. 2017.

[3] J. Q. James and A. Y. S. Lam, "Autonomous vehicle logistic system: Joint routing and charging strategy," *IEEE Trans. Intell. Transp.*, vol. 19, no. 7, pp. 2175–2187, Jul. 2018, doi: 10.1109/TITS.2017.2766682.

[4] J. Ji, A. Khajepour, W. W. Melek, and Y. Huang, "Path planning and tracking for vehicle collision avoidance based on model predictive control with multiconstraints," *IEEE Trans. Veh. Technol.*, vol. 66, no. 2, pp. 952–964, Feb. 2017.
[5] H. Guo, J. Liu, D. Cao, H. Chen, R. Yu, and C. Lv, "Dual-envelop-oriented moving horizon path tracking control for fully automated vehicles," *Mechatronics*, vol. 50, pp. 422–433, Apr. 2018, doi: 10.1016/j.mechatronics.2017.02.001.
[6] C.-L. Hwang, C.-C. Yang, and J. Y. Hung, "Path tracking of an autonomous ground vehicle with different payloads by hierarchical improved fuzzy dynamic sliding-mode control," *IEEE Trans. Fuzzy Syst.*, vol. 26, no. 2, pp. 899–914, Apr. 2018, doi: 10.1109/TFUZZ.2017.2698370.
[7] H. Jiang and Y. Q. Liang, "Online path planning of autonomous UAVs for bearing-only standoff multi-target following in threat environment," *IEEE Access*, vol. 6, pp. 22531–22544, 2018.
[8] M. M. G. Plessen and A. Bemporad, "Reference trajectory planning under constraints and path tracking using linear time-varying model predictive control for agricultural machines," *Biosyst. Eng.*, vol. 153, pp. 28–41, Jan. 2017.
[9] S. Liu, C. Xu, and L. Zhang, "Hierarchical robust path following control of fully submerged hydrofoil vessels," *IEEE Access*, vol. 5, pp. 21472–21487, 2017.
[10] X. Ji, Y. Liu, X. He, K. Yang, X. Na, C. Lv, and Y. Liu, "Interactive control paradigm-based robust lateral stability controller design for autonomous automobile path tracking with uncertain disturbance: A dynamic game approach," *IEEE Trans. Veh. Technol.*, vol. 67, no. 8, pp. 6906–6920, Aug. 2018.
[11] N. Wang, Z. Sun, J. Yin, S. F. Su, and S. Sharma, "Finite-time observer based guidance and control of underactuated surface vehicles with unknown sideslip angles and disturbances," *IEEE Access*, vol. 6, pp. 14059–14090, 2018.
[12] J. Taghia, X. Wang, S. Lam, and J. Katupitiya, "A sliding mode controller with a nonlinear disturbance observer for a farm vehicle operating in the presence of wheel slip," *Auton. Robots*, vol. 41, no. 1, pp. 71–88, Jan. 2017.
[13] A. A. Janbakhsh, M. B. Khaknejad, and R. Kazemi, "Simultaneous vehicle-handling and path-tracking improvement using adaptive dynamic surface control via a steer-by-wire system," *Proc. Inst. Mech. Eng., D, J. Automobile Eng.*, vol. 227, no. 3, pp. 345–360, Aug. 2012.
[14] S. A. Tchenderli-Braham, F. Hamerlain, and N. Saadia, "Experimentations on the adaptive sliding mode control for a trajectory tracking applied on a bi-steerable car," *Int. J. Vehicle Des.*, vol. 69, nos. 1–4, pp. 285–303, 2015.
[15] P. Hang and X. Chen, "Integrated chassis control algorithm design for path tracking based on four-wheel steering and direct yaw-moment control," *Proc. Inst. Mech. Eng., I, J. Syst. Control Eng.*, pp. 1–17, Oct. 2018. doi: 10.1177/0959651818806075.
[16] A. Gray, Y. Gao, J. K. Hedrick, and F. Borrelli, "Robust predictive control for semi-autonomous vehicles with an uncertain driver model," in *Proc. IEEE Intell. Vehicle Symp.*, Gold Coast, QLD, Australia, Jun. 2013, pp. 208–213.
[17] Y. Cai, Q. Zhan, and X. Xi, "Path tracking control of a spherical mobile robot," *Mech. Mach. Theory*, vol. 51, pp. 58–73, May 2012.
[18] J. Backman, T. Oksanen, and A. Visala, "Navigation system for agricultural machines: Nonlinear model predictive path tracking," *Comput. Electron. Agricult.*, vol. 82, pp. 32–43, May 2012.
[19] P. Hang, X. Chen, F. Luo, and S. Fang, "Robust control of a four-wheel-independent-steering electric vehicle for path tracking," *SAE Int. J. Veh. Dyn., Stab. NVH*, vol. 1, no. 2, pp. 307–316, Jul. 2017.
[20] C. Hu, R. Wang, F. Yan, and N. Chen, "Output constraint control on path following of four-wheel independently actuated autonomous ground vehicles," *IEEE Trans. Veh. Technol.*, vol. 65, no. 6, pp. 4033–4043, Jun. 2016.
[21] C. J. Ostafew, A. P. Schoellig, and T. D. Barfoot, "Robust constrained learning-based NMPC enabling reliable mobile robot path tracking," *Int. J. Robot. Res.*, vol. 35, no. 13, pp. 1547–1563, 2016.
[22] Y. Yoon, J. Shin, H. J. Kim, Y. Park, and S. Sastry, "Model-predictive active steering and obstacle avoidance for autonomous ground vehicles," *Control Eng. Pract.*, vol. 17, no. 7, pp. 741–750, Jul. 2009.
[23] G. Yin, J. Li, X. Jin, C. Bian, and N. Chen, "Integration of motion planning and model-predictive-control-based control system for autonomous electric vehicles," *Transport*, vol. 30, no. 3, pp. 353–360, Oct. 2015.
[24] T. Oda, K. Nonaka, and K. Sekiguchi, "Robust path tracking control using model predictive control and sliding mode control—Application to the JSAE-SICE benchmark problem," in *Proc. 54th Annu. Conf. Soc. Instrum. Control Eng. Japan (SICE)*, Jul. 2015, pp. 1332–1336.
[25] C. Lian, X. Xu, H. Chen, and H. He, "Near-optimal tracking control of mobile robots via receding-horizon dual heuristic programming," *IEEE Trans. Cybern.*, vol. 46, no. 11, pp. 2484–2496, Nov. 2016.
[26] L. Wang, "Discrete-time MPC using laguerre function," in *Model Predictive Control System Design and Implementation Using MATLAB*, M. J. Grimble, Ed. London, U.K.: Springer, 2009, pp. 85–148.
[27] L. Wang, "Use of exponential data weighting in model predictive control design," in *Proc. 40th IEEE Conf. Decis. Control*, Orlando, FL, USA, Dec. 2001, pp. 4857–4862.
[28] J. Guo, Y. Luo, and K. Li, "An adaptive hierarchical trajectory following control approach of autonomous four-wheel independent drive electric vehicles," *IEEE Trans. Intell. Transp. Syst.*, vol. 19, no. 8, pp. 2482–2492, Aug. 2018.
[29] K. Worthmann, M. Reble, L. Grüne, and F. Allgöwer, "The role of sampling for stability and performance in unconstrained nonlinear model predictive control," *SIAM J. Control Optim.*, vol. 52, no. 1, pp. 581–605, Feb. 2014.
[30] S.-K. Oh, B. J. Park, and J. M. Lee, "Point-to-point iterative learning model predictive control," *Automatica*, vol. 89, pp. 135–143, Mar. 2018.
[31] J. Nilsson, J. Fredriksson, and A. C. E. Ödblom, "Reliable vehicle pose estimation using vision and a single-track model," *IEEE Trans. Intell. Transp. Syst.*, vol. 15, no. 6, pp. 2630–2643, Dec. 2014.
[32] B. Gutjahr, L. Gröll, and M. Werling, "Lateral vehicle trajectory optimization using constrained linear time-varying MPC," *IEEE Trans. Intell. Transp. Syst.*, vol. 18, no. 6, pp. 1586–1595, Jun. 2017.
[33] P. Falcone, F. Borrelli, J. Asgari, H. E. Tseng, and D. Hrovat, "Predictive active steering control for autonomous vehicle systems," *IEEE Trans. Control Syst. Technol.*, vol. 15, no. 3, pp. 566–580, May 2007.
[34] S. Sakai, H. Sado, and Y. Hori, "Dynamic driving/braking force distribution in electric vehicles with independently driven four wheels," *Elect. Eng. Jpn.*, vol. 138, no. 1, pp. 79–89, Jan. 2002.
[35] B. Ren, H. Chen, H. Zhao, and L. Yuan, "MPC-based yaw stability control in in-wheel-motored EV via active front steering and motor torque distribution," *Mechatronics*, vol. 38, pp. 103–114, Sep. 2016.
[36] M. N. Zeilinger, M. Morari, and C. N. Jones, "Soft constrained model predictive control with robust stability guarantees," *IEEE Trans. Autom. Control*, vol. 59, no. 5, pp. 1190–1202, May 2014.
[37] P. Falcone, F. Borrelli, J. Asgari, E. H. Tseng, and D. Hrovat, "Linear time-varying model predictive control and its application to active steering systems: Stability analysis and experimental validation," *Int. J. Robust Nonlinear Control*, vol. 21, no. 8, pp. 943–944, May 2011.
[38] L. Wang, "Discrete model predictive controller design using Laguerre functions," *J. Process Control*, vol. 14, no. 2, pp. 131–142, Mar. 2004.
[39] T. T. V. Yap, A. H. Tan, and W. N. Tan, "Identification of higher-dimensional ill-conditioned systems using extensions of virtual transfer function between inputs," *J. Process Control*, vol. 56, pp. 58–68, Aug. 2017.
[40] N. Emmart, Y. Chen, and C. C. Weems, "Computing the smallest eigenvalue of large ill-conditioned Hankel matrices," *Commun. Comput. Phys.*, vol. 18, no. 1, pp. 104–124, Jul. 2015.
[41] P. Song, M. Tomizuka, and C. Zong, "A novel integrated chassis controller for full drive-by-wire vehicles," *Vehicle Syst. Dyn., Int. J. Vehicle Mech. Mobility*, vol. 53, no. 2, pp. 215–236, 2015.

BING ZHANG received the B.Eng. degree from the Humanities and Information College, Changchun University of Technology, Changchun, China, in 2012, and the M.Eng. degree from the Changchun University of Technology, in 2015. She is currently pursuing the Ph.D. degree with the Department of State Key Laboratory of Automotive Simulation and Control, Jilin University, Changchun.

Her research interests include control-by-wire vehicle control, autonomous vehicle control, and vehicle dynamic stability control.

CHANGFU ZONG received the B.Eng. degree from the Liaoning University of Technology, Jinzhou, China, in 1986, and the M.Eng. and Ph.D. degrees from the Jilin University of Technology, Changchun, China, in 1994 and 1998, respectively.

He is currently a Professor with the Department of State Key Laboratory of Automotive Simulation and Control, Jilin University, Changchun. He has been an Academic Visitor with Cambridge University, U.K, in 2005, and a Senior Academic Visitor with the University of California at Berkeley, USA, in 2013. He has published over 200 articles. His research interests include vehicle control stability, new energy vehicles, and autonomous vehicle control.

GUOYING CHEN received the B.Eng. degree from China Agricultural University, Beijing, China, in 2005, the M.Eng. degree from Xinhua University, Chengdu, China, in 2009, and the Ph.D. degree from the Jilin University of Technology, Changchun, China, in 2012.

He is currently a Professor with the Department of State Key Laboratory of Automotive Simulation and Control, Jilin University, Changchun. His research interests include vehicle dynamics simulation and control.

BANGCHENG ZHANG received the B.Eng. and M.Eng. degrees from the Changchun University of Technology, Changchun, China, in 1995 and 2004, respectively, and the Ph.D. degree from Jilin University, Changchun, in 2011.

He is currently a Professor with the Changchun University of Technology. He has been an Academic Visitor with Tsinghua University, Beijing, China, in 2007. He has published over 20 articles. His research interests include mechatronics measurement technique and fault diagnosis.